

ULTRASONIC TREATMENT WITH NICKEL ELECTROPLATING COMBINED  
WITH OXIDATION FOR DEVELOPING  $\gamma$ -Al<sub>2</sub>O<sub>3</sub> WASHCOAT ON Fe-Cr-Al  
SUBSTRATE

ADE FIRDIANTO

A thesis submitted in fulfillment of the requirement for the award of the  
Degree of Master of Mechanical Engineering

Faculty of Mechanical and Manufacturing Engineering  
Universiti Tun Hussein Onn Malaysia

FEBRUARY 2012

## ABSTRACT

Fe-Cr-Al is used as metallic support for catalytic converter due to its high thermal conductivity, lower heat capacity, high temperature and mechanical shock resistance.  $\gamma$ -Al<sub>2</sub>O<sub>3</sub> is the most widely used material as washcoat which embedded on metallic support for the catalytic converter application. The problem is the coating adhesion between the metallic support and the ceramic washcoat becomes a problem in long-term high temperature oxidation. On the other hand, the gamma phase of alumina will be transformed to alpha phase at high temperature. The ultrasonic technique via cavitation bubbles and high velocity can make surface deformation and also accelerate the  $\gamma$ -Al<sub>2</sub>O<sub>3</sub> powders to bombardment occurred on the Fe-Cr-Al surface. This process generates sufficiently heat and  $\gamma$ -Al<sub>2</sub>O<sub>3</sub> layer can be formed on the Fe-Cr-Al surface. Subsequently, electroplating process embeds the nickel and also can strengthen the adhesion when oxidized. Therefore, this work presents the ultrasonic treatment with nickel electroplating for developing  $\gamma$ -Al<sub>2</sub>O<sub>3</sub> washcoat on Fe-Cr-Al substrate and oxidation treatment for catalytic converter application. Washcoat layer on Fe-Cr-Al was prepared by using  $\gamma$ -Al<sub>2</sub>O<sub>3</sub> powders through ultrasonic treatment. Catalyst material was prepared by using nickel electroplating. The oxidation kinetics was conducted at temperatures of 500, 700, 900 and 1100 °C in air for 100 hours. The surface morphology, cross section analysis, chemical composition, elemental maps and phase structure of coated Fe-Cr-Al were analyzed by Scanning Electron Microscope (SEM), Energy Dispersive X-ray Spectroscopy (EDS) and X-ray Diffraction (XRD) respectively. The results showed that the surface of Fe-Cr-Al contained  $\gamma$ -Al<sub>2</sub>O<sub>3</sub> powders after ultrasonic treatment. The layer of alumina oxide has been formed on coated Fe-Cr-Al and no spallation occurred after oxidation. It is prove that  $\gamma$ -Al<sub>2</sub>O<sub>3</sub> washcoat and NiO as a catalyst have successfully embedded on Fe-Cr-Al substrate by ultrasonic treatment combined with nickel electroplating at long term high temperature oxidation that enhance the adhesive properly.

## ABSTRAK

Fe-Cr-Al digunakan sebagai sokongan logam untuk penukar bermangkin. Secara umumnya,  $\gamma$ -Al<sub>2</sub>O<sub>3</sub> adalah bahan yang digunakan sebagai *washcoat* yang dilekatkan pada sokongan logam untuk aplikasi penukar bermangkin. Masalahnya ialah, lekatan lapisan antara sokongan logam dan seramik *washcoat* menjadi masalah dalam pengoksidaan suhu tinggi bagi satu jangka masa yang lama. Selain daripada itu, fasa gamma alumina akan mengalami transformasi ke alpha pada suhu tinggi. Teknik ultrasonik melalui gelembung kaviti dan kelajuan tinggi akan menyebabkan deformasi permukaan dan juga boleh mempercepatkan serbuk  $\gamma$ -Al<sub>2</sub>O<sub>3</sub> menyentuh permukaan Fe-Cr-Al. Proses ini menghasilkan haba yang mencukupi dan lapisan  $\gamma$ -Al<sub>2</sub>O<sub>3</sub> boleh terbentuk pada permukaan Fe-Cr-Al. Disamping melekatkan nikel, proses penyaduran juga boleh menguatkan lekatan ketika dioksida. Oleh kerana itu dalam kajian ini, kaedah rawatan ultrasonik dengan penyaduran nikel untuk pengembangan  $\gamma$ -Al<sub>2</sub>O<sub>3</sub> sebagai *washcoat* pada substrat Fe-Cr-Al dan rawatan pengoksidaan untuk aplikasi penukar bermangkin. Lapisan *washcoat* pada Fe-Cr-Al disusun dengan menggunakan serbuk  $\gamma$ -Al<sub>2</sub>O<sub>3</sub> melalui kaedah rawatan ultrasonik. Bahan pemangkin disediakan dengan menggunakan nikel melalui proses penyaduran. Pengoksidaan dilakukan di antara suhu 500, 700, 900 dan 1100 °C di udara selama 100 jam. Morfologi permukaan, keratan rentas, komposisi kimia, pemetaan elemen dan struktur fasa dianalisis menggunakan Scanning Electron Microscope (SEM), Energy Dispersive X-ray Spectroscopy (EDS) dan X-ray Diffraction (XRD). Keputusan yang diperolehi menunjukkan bahawa pada permukaan Fe-Cr-Al mengandungi lapisan serbuk  $\gamma$ -Al<sub>2</sub>O<sub>3</sub> selepas rawatan ultrasonik. Lapisan alumina oksida terbentuk pada permukaan Fe-Cr-Al dan pengelupasan tidak berlaku selepas pengoksidaan. Ini membuktikan bahawa *washcoat*  $\gamma$ -Al<sub>2</sub>O<sub>3</sub> dan NiO sebagai pemangkin berjaya melekat pada substrat Fe-Cr-Al melalui rawatan ultrasonik yang digabungkan dengan penyaduran nikel pada pengoksidaan suhu tinggi bagi jangka masa yang lama dan dapat meningkatkan lekatan dengan baik.

**CONTENTS**

<b>TITLE</b>	<b>i</b>
<b>DECLARATION</b>	<b>ii</b>
<b>DEDICATION</b>	<b>iii</b>
<b>ACKNOWLEDGEMENT</b>	<b>iv</b>
<b>ABSTRACT</b>	<b>v</b>
<b>CONTENTS</b>	<b>vii</b>
<b>LIST OF TABLES</b>	<b>xiii</b>
<b>LIST OF FIGURES</b>	<b>xiv</b>
<b>LIST OF SYMBOLS AND ABBREVIATIONS</b>	<b>xx</b>
<b>LIST OF APPENDIX</b>	<b>xxiv</b>
<b>CHAPTER 1 INTRODUCTION</b>	<b>1</b>
1.1 Background of Study	1
1.2 Problem Statements	3

1.3	Hypothesis	4
1.4	Aim of Study	4
1.5	Objective of Study	4
1.6	Scope of Study	5
<b>CHAPTER 2 LITERATURE REVIEW</b>		<b>6</b>
2.1	Catalytic Converter	6
2.1.1	Substrate	8
2.1.1.1	Metallic Substrate	9
2.1.1.2	Fe-Cr-Al Metallic Substrate	11
2.2	Washcoat	12
2.2.1	Al <sub>2</sub> O <sub>3</sub> Washcoat	13
2.3	Particle Size Distribution of the Carrier/Washcoat	15
2.4	Washcoat Development on Fe-Cr-Al Metallic Substrate	16
2.5	Catalyst Material for Catalytic Converter	18
2.5.1	Nickel as Catalyst Material	18

2.6	Ultrasonic Surface Treatment	19
2.6.1	Reactions Involving Metal or Solid Surfaces	20
2.6.2	Reactions Involving Powders or Other Particulate Matter	20
2.7	Acoustic Cavitation	21
2.7.1	Cavitation Near a Surface	22
2.7.2	Heterogeneous Powder Liquid Reactions	23
2.8	Nickel Electroplating	25
2.8.1	Basic Process of Electrodeposition	25
2.8.2	Sulphamate Nickel Electroplating Solutions	27
2.8.3	Average Coating Coverage	28
2.9	Oxidation of Fe-Cr-Al Coating	29
2.9.1	Wagner's Oxidation Theory	30
2.9.2	Oxidation Related to Catalytic Materials	32
2.9.3	Transient Behaviour Associated with Alumina Phase Transformations	34

<b>CHAPTER 3 METHODOLOGY</b>	<b>36</b>
3.1 Catalysis Material and Substrate	36
3.2 Material Preparation	37
3.2.1 Ultrasonic Treatment of $\gamma$ -Al <sub>2</sub> O <sub>3</sub> Powder	37
3.2.2 Particle Size Analysis and Distribution of $\gamma$ -Al <sub>2</sub> O <sub>3</sub> After Sonicated by Ultrasonic Clamp-on Tubular Reactor	38
3.3 Experimental Procedures	40
3.3.1 Ultrasonic Treatment of Fe-Cr-Al Foils mixed with $\gamma$ -Al <sub>2</sub> O <sub>3</sub> Powder	40
3.3.2 Nickel Electroplating	41
3.3.3 Oxidation of Coated Fe-Cr-Al	43
3.4 Characterization	43
3.4.1 Scanning Electron Microscopy (SEM) and Energy Dispersive X-ray Spectroscopy (EDS)	45
3.4.2 X-ray Diffraction (XRD)	46

<b>CHAPTER 4 RESULT AND DISCUSSION</b>	<b>49</b>
4.1 Effect of Ultrasonic Treatment Period on the $\gamma$ -Al <sub>2</sub> O <sub>3</sub> Powder in Term of Particle Size and Distribution	49
4.1.1 Microstructure Observation of $\gamma$ -Al <sub>2</sub> O <sub>3</sub> Powder Pre and Post Ultrasonic Treatment	52
4.1.2 Phase Analysis of $\gamma$ -Al <sub>2</sub> O <sub>3</sub> After Ultrasonic Treatment	55
4.2 Distribution of $\gamma$ -Al <sub>2</sub> O <sub>3</sub> Powder on Fe-Cr-Al Surface After Ultrasonic Treatment	56
4.3 Oxidation of coated Fe-Cr-Al	58
4.3.1 Weight Gain of coated Fe-Cr-Al	58
4.3.2 Comparison of Weight Gain of Coated Fe-Cr-Al by Ultrasonic Treatment with $\gamma$ -Al <sub>2</sub> O <sub>3</sub> and Al <sub>2</sub> O <sub>3</sub> Oxidized at 900 °C and 1100 °C	61
4.3.2.1 Comparison of Weight Gain of Coated Fe-Cr-Al by Ultrasonic Treatment with $\gamma$ -Al <sub>2</sub> O <sub>3</sub> and Al <sub>2</sub> O <sub>3</sub> Oxidized at 900 °C for 100 Hours	62
4.3.2.2 Comparison of Weight Gain of Coated Fe-Cr-Al by Ultrasonic Treatment with $\gamma$ -Al <sub>2</sub> O <sub>3</sub> and Al <sub>2</sub> O <sub>3</sub> Oxidized at 1100 °C for 100 Hours	66
4.3.3 Parabolic Rate Constant ( $k_p$ ) of coated Fe-Cr-Al	71



4.4	Phase analysis of Coated Fe-Cr-Al After Oxidation at Temperatures of 500, 700, 900 and 1100 °C	75
4.5	Surface Morphology of Coated Fe-Cr-Al After Oxidation at Temperatures of 500, 700, 900 and 1100 °C	77
4.6	Cross-section and EDS Chemical Analysis of $\gamma$ -Al <sub>2</sub> O <sub>3</sub> Washcoat on Fe-Cr-Al After Oxidation at Temperature of 900 °C and 1100 °C	85
<b>CHAPTER 5 CONCLUSION AND FUTURE WORK</b>		<b>89</b>
5.1	Conclusion	89
5.2	Future Work	90
<b>REFERENCES</b>		<b>91</b>
<b>APPENDICES</b>		<b>97</b>
<b>VITA</b>		

**LIST OF TABLES**

2.1	Typical composition of electroplating solutions and electroplating parameter	27
2.2	Time to electrodeposit nickel at various current densities	29
3.1	Chemical composition ( <i>wt.%</i> ) of Fe-Cr-Al foil	36
3.2	Process condition for clamp-on tubular reactor	38
3.3	Fe-Cr-Al treatment conditions	40
3.4	Chemical composition of electrolyte	42
4.1	Parabolic rate constant ( $k_p$ ) of all coated Fe-Cr-Al after oxidation at range of 500 °C to 1100 °C	74
4.2	EDS composition point (01, 02 and 03) analysis data at 900 °C	86
4.3	EDS composition point (01, 02 and 03) analysis data at 1100 °C	87

## LIST OF FIGURES

1.1	The focused area on washcoat and catalyst development for catalytic converter	3
2.1	Structure of catalytic converter	7
2.2	Parameters affecting on the catalyst performance	8
2.3	The design of metallic monolith substrate	11
2.4	Schematic diagram for catalytic sites dispersed on a high surface area of $\text{Al}_2\text{O}_3$ carrier bonded to a monolith support	13
2.5	(a) Scanning electron microscope (SEM) image of gamma ( $\gamma\text{-Al}_2\text{O}_3$ ), (b) SEM of alpha ( $\alpha\text{-Al}_2\text{O}_3$ )	14
2.6	Particle size measurement using CILAS particle size analyzer (PSA)	16
2.7	Generation of an acoustic bubble	22
2.8	Cavitation bubble collapse at or near a solid surface	23
2.9	Acoustic cavitation in a liquid with a suspended powder	24
2.10	Cavitation effects in a heterogeneous liquid system	24
2.11	Basic electrical circuit for electroplating	25
2.12	Schematic process for the protective oxide scale during the initial and transient oxidation stage	30
2.13	Hypothetical mass-gain versus time curve for an oxidation reaction	31
2.14	The temperature profile of inlet/outlet gas and substrate for 500 second test cycle	32
2.15	A variation of $\text{Al}_2\text{O}_3$ transformation temperature on bulk material used for catalyst supports (a) $\gamma\text{-Al}_2\text{O}_3 + 3\% \text{Pt}$ (b) $\gamma\text{-Al}_2\text{O}_3$	34

3.1	Equipment of ultrasonic clamp-on tubular reactor	37
3.2	CILAS 1180 particles size analyzer	38
3.3	Schematic diagram of CILAS 1180 particle size analyzer work	39
3.4	Schematic diagram of ultrasonic treatment process using laborette 17 ultrasonic cleaning bath	41
3.5	Schematic diagram of electroplating process	42
3.6	Cyclic oxidation of coated Fe-Cr-Al at temperature of 900 °C for 100 hours. Similar cyclic approaches were applied to 500, 700 and 1100 °C	43
3.7	(a) Hand grinder instrument and (b) polishing machine	44
3.8	Scanning Electron Microscopy (SEM) attached with Energy Dispersive X-ray Spectroscopy (EDS)	45
3.9	X-ray Diffraction (XRD) Bruker D8-Advance	46
3.10	The conditions required for constructive interference determined by Bragg's Law	47
3.11	Notation of lattice points, rows and planes	48
4.1	Particles size and distribution of raw material $\gamma$ -Al <sub>2</sub> O <sub>3</sub> powder	50
4.2	Particles size and distribution of $\gamma$ -Al <sub>2</sub> O <sub>3</sub> powder after ultrasonic for 10 minutes	50
4.3	Particles size and distribution of $\gamma$ -Al <sub>2</sub> O <sub>3</sub> powder after ultrasonic for 20 minutes	51
4.4	Particles size and distribution of $\gamma$ -Al <sub>2</sub> O <sub>3</sub> powder after ultrasonic for 30 minutes	52
4.5	SEM image of raw material $\gamma$ -Al <sub>2</sub> O <sub>3</sub> powders	53
4.6	SEM image of $\gamma$ -Al <sub>2</sub> O <sub>3</sub> powders after ultrasonic for 10 minutes	53

4.7	SEM image of $\gamma$ -Al <sub>2</sub> O <sub>3</sub> powders after ultrasonic for 20 minutes	54
4.8	SEM image of $\gamma$ -Al <sub>2</sub> O <sub>3</sub> powders (a) after ultrasonic for 30 minutes and (b) $\gamma$ -Al <sub>2</sub> O <sub>3</sub> agglomerate at higher magnification	54
4.9	XRD pattern of $\gamma$ -Al <sub>2</sub> O <sub>3</sub> powder after sonication for 30 minutes	55
4.10	Surface morphology and chemical composition of the Fe-Cr-Al substrate (a), and the effect of $\gamma$ -Al <sub>2</sub> O <sub>3</sub> after ultrasonic treatment within (b) 10, (c) 20, (d) 30, (e) 40 and (f) 50 minutes	57
4.11	Weight gain vs. oxidation time at 500 °C for Fe-Cr-Al treated with $\gamma$ -Al <sub>2</sub> O <sub>3</sub> by ultrasonic in 10, 20, 30, 40 and 50 minutes	58
4.12	Weight gain vs. oxidation time at 700 °C for Fe-Cr-Al treated with $\gamma$ -Al <sub>2</sub> O <sub>3</sub> by ultrasonic in 10, 20, 30, 40 and 50 minutes	59
4.13	Weight gain vs. oxidation time at 900 °C for Fe-Cr-Al treated with $\gamma$ -Al <sub>2</sub> O <sub>3</sub> by ultrasonic in 10, 20, 30, 40 and 50 minutes	60
4.14	Weight gain vs. oxidation time at 1100 °C for Fe-Cr-Al treated with $\gamma$ -Al <sub>2</sub> O <sub>3</sub> by ultrasonic in 10, 20, 30, 40 and 50 minutes	61
4.15	Comparison of weight gain of Fe-Cr-Al treated under 10 minutes ultrasonic treatment for $\gamma$ -Al <sub>2</sub> O <sub>3</sub> and Al <sub>2</sub> O <sub>3</sub> surface after oxidation at 900 °C for 100 hours	62

- 4.16 Comparison of weight gain of Fe-Cr-Al treated under 20 minutes ultrasonic treatment for  $\gamma$ -Al<sub>2</sub>O<sub>3</sub> and Al<sub>2</sub>O<sub>3</sub> surface after oxidation at 900 °C for 100 hours 63
- 4.17 Comparison of weight gain of Fe-Cr-Al treated under 30 minutes ultrasonic treatment for  $\gamma$ -Al<sub>2</sub>O<sub>3</sub> and Al<sub>2</sub>O<sub>3</sub> surface after oxidation at 900 °C for 100 hours 64
- 4.18 Comparison of weight gain of Fe-Cr-Al treated under 40 minutes ultrasonic treatment for  $\gamma$ -Al<sub>2</sub>O<sub>3</sub> and Al<sub>2</sub>O<sub>3</sub> surface after oxidation at 900 °C for 100 hours 65
- 4.19 Comparison of weight gain of Fe-Cr-Al treated under 50 minutes ultrasonic treatment for  $\gamma$ -Al<sub>2</sub>O<sub>3</sub> and Al<sub>2</sub>O<sub>3</sub> surface after oxidation at 900 °C for 100 hours 65
- 4.20 Comparison of weight gain of Fe-Cr-Al treated under 10 minutes ultrasonic treatment for  $\gamma$ -Al<sub>2</sub>O<sub>3</sub> and Al<sub>2</sub>O<sub>3</sub> surface after oxidation at 1100 °C for 100 hours 66
- 4.21 Comparison of weight gain of Fe-Cr-Al treated under 20 minutes ultrasonic treatment for  $\gamma$ -Al<sub>2</sub>O<sub>3</sub> and Al<sub>2</sub>O<sub>3</sub> surface after oxidation at 1100 °C for 100 hours 67
- 4.22 Comparison of weight gain of Fe-Cr-Al treated under 30 minutes ultrasonic treatment for  $\gamma$ -Al<sub>2</sub>O<sub>3</sub> and Al<sub>2</sub>O<sub>3</sub> surface after oxidation at 1100 °C for 100 hours 68

- 4.23 Comparison of weight gain of Fe-Cr-Al treated under 40 minutes ultrasonic treatment for  $\gamma$ -Al<sub>2</sub>O<sub>3</sub> and Al<sub>2</sub>O<sub>3</sub> surface after oxidation at 1100 °C for 100 hours 69
- 4.24 Comparison of weight gain of Fe-Cr-Al treated under 50 minutes ultrasonic treatment for  $\gamma$ -Al<sub>2</sub>O<sub>3</sub> and Al<sub>2</sub>O<sub>3</sub> surface after oxidation at 1100 °C for 100 hours 70
- 4.25 Parabolic rate constant ( $k_p$ ) value at temperature 500 °C for Fe-Cr-Al treated with  $\gamma$ -Al<sub>2</sub>O<sub>3</sub> by ultrasonic in 10, 20, 30, 40 and 50 minutes 71
- 4.26 Parabolic rate constant ( $k_p$ ) value at temperature 700 °C for Fe-Cr-Al treated with  $\gamma$ -Al<sub>2</sub>O<sub>3</sub> by ultrasonic in 10, 20, 30, 40 and 50 minutes 72
- 4.27 Parabolic rate constant ( $k_p$ ) value at temperature 900 °C for Fe-Cr-Al treated with  $\gamma$ -Al<sub>2</sub>O<sub>3</sub> by ultrasonic in 10, 20, 30, 40 and 50 minutes 73
- 4.28 Parabolic rate constant ( $k_p$ ) value at temperature 1100 °C for Fe-Cr-Al treated with  $\gamma$ -Al<sub>2</sub>O<sub>3</sub> by ultrasonic in 10, 20, 30, 40 and 50 minutes 74
- 4.29 The phase analysis of coated Fe-Cr-Al after oxidation (a) 500, (b) 700, (c) 900 and (d) 1100 °C for 100 hours 76
- 4.30 Surface morphology and chemical composition of Fe-Cr-Al treated with  $\gamma$ -Al<sub>2</sub>O<sub>3</sub> by ultrasonic with time variation of (a) 10, (b) 20, (c) 30, (d) 40 and (e) 50 minutes and oxidized at 500 °C for 100 hours 78

4.31	Surface morphology and chemical composition of Fe-Cr-Al treated with $\gamma$ -Al <sub>2</sub> O <sub>3</sub> by ultrasonic with time variation of (a) 10, (b) 20, (c) 30, (d) 40 and (e) 50 minutes and oxidized at 700 °C for 100 hours	80
4.32	Surface morphology and chemical composition of Fe-Cr-Al treated with $\gamma$ -Al <sub>2</sub> O <sub>3</sub> by ultrasonic with time variation of (a) 10, (b) 20, (c) 30, (d) 40 and (e) 50 minutes and oxidized at 900 °C for 100 hours	82
4.33	Surface morphology and chemical composition of Fe-Cr-Al treated with $\gamma$ -Al <sub>2</sub> O <sub>3</sub> by ultrasonic with time variation of (a) 10, (b) 20, (c) 30, (d) 40 and (e) 50 minutes and oxidized at 1100 °C for 100 hours	84
4.34	Lateral cross-section analysis of coated Fe-Cr-Al at 900 °C	85
4.35	Lateral cross-section analysis of coated Fe-Cr-Al at 1100 °C	86
4.36	EDS elemental maps analysis at lateral view of $\gamma$ -Al <sub>2</sub> O <sub>3</sub> layer on coated Fe-Cr-Al at 900 °C	87
4.37	EDS elemental maps analysis at lateral view of $\gamma$ -Al <sub>2</sub> O <sub>3</sub> layer on coated Fe-Cr-Al at 1100 °C	88



## LIST OF SYMBOLS AND ABBREVIATIONS

$\text{Al}_2\text{O}_3$	-	Aluminum Oxide
Fe-Cr-Al	-	Iron-Chromium-Aluminium
$^{\circ}\text{C}$	-	Degree Celsius
NiO	-	Nickel Oxide
CO	-	Carbon monoxide
$\text{NO}_x$	-	Nitrogen Oxide
HC	-	Hydrocarbons
%	-	Percent
$k_p$	-	Parabolic Rate Contant
$\text{N}_2$	-	Nitrogen
$\text{CO}_2$	-	Carbon Dioxide
$\text{H}_2\text{O}$	-	Dihydrogen Monoxide (Water)
$\text{O}_2$	-	Oxygen
$\mu\text{m}$	-	Micrometer
cm	-	Centimeter
mm	-	Millimeter
mil	-	Mile
cpsi	-	Cells Per Square Inch
inch	-	Inchies
$\alpha$	-	Alpha
$\gamma$	-	Gamma
$\theta$	-	Theta
$\delta$	-	Delta
$\eta$	-	Eta
wt	-	Weight
Al	-	Aluminum
RE	-	Reactive Element

Mg	-	Magnesium
Mo	-	Molybdenum
Mn	-	Manganese
Co	-	Cobalt
Cu	-	Copper
Zr	-	Zirconium
Y	-	Yttrium
Ce	-	Cerium
La	-	Lanthanum
Hf	-	Hafnium
$m^2$	-	Meter Square
$g$	-	Gram
$\mu$	-	Micron
Ni	-	Nickel
Pt	-	Platinum
Pd	-	Palladium
Rh	-	Rhodium
H <sub>2</sub> S	-	Hydrogen Sulfide
Hz	-	Hertz
kHz	-	Kilohertz
MHz	-	Megahertz
$K$	-	Mass Transfer Coefficient
$A$	-	Surface Area
$T$	-	Average Thickness
$I$	-	Current
$t$	-	Time
$dm^2$	-	Decimeter Square
$W_t$	-	Weight After Oxidation
$W_o$	-	Initial Weight
$W(t)$	-	Weight Gain

J	-	Current Density
W	-	Watt
V	-	Volt
kg	-	Kilogram
L	-	Liter
HCl	-	Hydrochloric Acid
NaOH	-	Sodium Hydroxide
$\text{Ni}(\text{SO}_3\text{NH}_2)_2 \cdot 4\text{H}_2\text{O}$	-	Nickel Sulphamate
$\text{NiCl} \cdot 6\text{H}_2\text{O}$	-	Nickel Chloride
$\text{H}_2\text{BO}_3$	-	Boric Acid
$\text{C}_{12}\text{H}_{25}\text{SO}_4\text{Na}$	-	Sodium Lauryal Sulphate
A	-	Ampere
SiC	-	Silicon Carbide
Q3	-	Cummulative Value
q3	-	Population Density
x	-	Particle Diameter
C	-	Carbon
min	-	Minutes
h	-	Hour
ASTM	-	American Society For Testing and Materials
BES	-	Back Scattered
EBSD	-	Electron Backscattered Diffraction
EDS	-	Energy Dispersive X-ray Spectroscopy
EPA	-	Environmental Protection Agency
GSA	-	Geometrical Surface Area
LEV II	-	Low Emission Vehicle II
PSA	-	Particle Size Analyzer
PSD	-	Particle Size Distribution
SEM	-	Scanning Electron Microscopy
SET	-	Single Electron Transfer

TWC	- Three-Way Catalyst
VOCs	- Volatile Organic Compounds
XRD	- X-ray Diffraction

**LIST OF APPENDICES**

<b>APPENDIX</b>	<b>TITLE</b>	<b>PAGE</b>
A	Generator Specification of Ultrasonic Clamp-On Tubular Reactor	97
B	Flowchart of Research Methodology	98
C	Particle Size Analyzer Data	99
D	Weight Gain Data	109
E	List of Publications	111

## CHAPTER 1

### INTRODUCTION

In this chapter, the background of this research will be explained in detail which consists of research background, problem statement, hypothesis, aim, objective and scope of study.

#### 1.1 Background of study

Air pollution caused by cars is one of the most challenging problems that contribute to the environment problem. By-products of the operation of the gasoline engine include carbon monoxide (CO), oxides of nitrogen (NO<sub>x</sub>), and unburned fuel compounds is hydrocarbons (HC), each of which is a pollutant (George, 2006). It is known that exhaust gas emissions from the vehicles can cause serious problems for human health and greenhouse effect that could endanger the world. Many automotive industries and research institutes have tried to develop catalytic converter technology (Zhao *et al.*, 2003).

The catalytic converter is a device incorporated into the exhaust system of an automobile that reduces the amount of pollutants in the automobile's exhaust gases. The centerpiece of this technology based on to the three-way catalyst (TWC) used on gasoline spark-ignited vehicles in all major world markets today. The name “three-way catalyst” was applied to catalytic controls that capable of reducing all three criteria pollutants such as, carbon monoxide (CO), oxides of nitrogen (NO<sub>x</sub>), and volatile organic compounds (VOCs). The three-way catalytic converter (TWC) has been the primary emission control technology on light-duty gasoline vehicles since the early 1980 (Kubsh, 2006). This device is located in-line with the exhaust system

and used to cause a desirable chemical reaction to take place in the exhaust flow. Today, more than 90% of the new automobiles sold around the world are equipped with catalytic converters.

The regulatory programs have been continually pushed to lower levels in response to air quality concerns. California was adopted Low Emission Vehicle II (LEV II) program in late 1998, followed by Environmental Protection Agency (EPA) finalizing the Tier 2 regulations in December 1999, Europe (Euro 3 and Euro 4 regulations), Japan (Japan Low Emission Vehicle regulations) and Korea (Korea Low Emission Vehicle regulations). Emission regulations for new vehicles based on the use of three-way catalyst technologies are now being implemented in almost every world market, including large emerging markets in India and China (Kubsh, 2006).

Fe-Cr-Al foils become the most popular material than ceramics in the fabrication of catalytic converter monolith due to its advantages for high temperature resistance. Fe-Cr-Al is also easily manufactured as honeycomb substrate with thinner walls, so that obtain a lower pressure drop and higher contact surface area (Wu *et al.*, 2005). Fe-Cr-Al was mentioned that the corrugated and spiral shaped tools have been successfully designed and developed for manufacturing the hand-made catalytic converter in full scale size (Fahrul *et al.*, 2009). The washcoat developments usually use deposition technique such as a precipitation and dip-coating method (Valentini *et al.*, 2001), by impregnation method (Betta, 1997), or electroplating method (Sebayang *et al.*, 2010). The most widely used material in the application of washcoat is  $\gamma$ -Al<sub>2</sub>O<sub>3</sub>.  $\gamma$ -Al<sub>2</sub>O<sub>3</sub> has a large surface area, good pore size distribution, surface acidic properties, composition of trace components and crystal structure (Heck *et al.*, 2009). Particle size influences the surface area on washcoat with the smaller of particle size increase the surface area compared with large particles in the same amount and that could affect the quality of washcoat (Ghosh *et al.*, 2008). The focused of research area is shown in Figure 1.1.

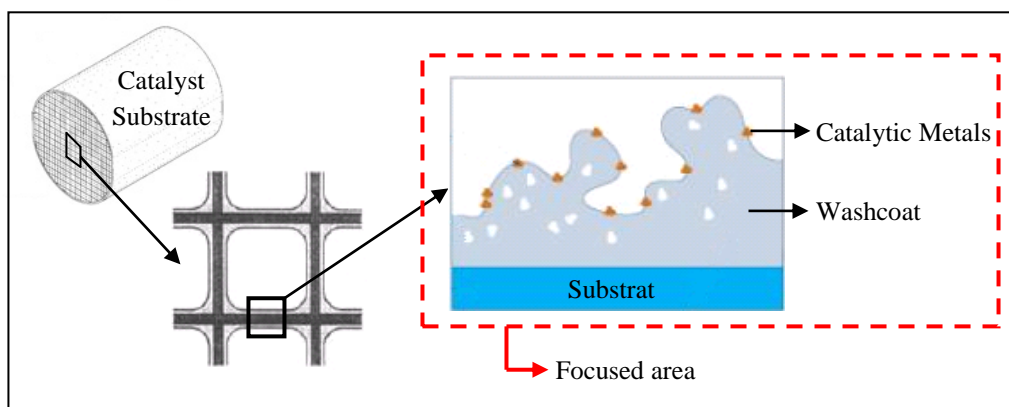


Figure 1.1: The focused area on washcoat and catalyst development for catalytic converter.

## 1.2 Problem statements

The coating adhesion between the metallic support and the ceramic washcoat becomes a problem in long-term oxidation between 900 °C and 1100 °C (Y. Putrasari, 2011). The adhesive ability of the washcoat was still difficult to ensure. The washcoat layer is peeling because of the loose adhesion and an unstable oxide growth in long term oxidation.  $\gamma\text{-Al}_2\text{O}_3$  will transformed into  $\alpha\text{-Al}_2\text{O}_3$  at higher temperatures. However,  $\alpha\text{-Al}_2\text{O}_3$  has a smaller of surface area and inappropriate for use as a washcoat. On the other hand, the characteristic of  $\gamma\text{-Al}_2\text{O}_3$  coated on the Fe-Cr-Al at low temperature between 500 °C and 700 °C had not been investigated. Therefore, this work will discussed on a fundamental study on utilization of  $\gamma\text{-Al}_2\text{O}_3$  as washcoat on Fe-Cr-Al metallic substrates by ultrasonic treatment with nickel electroplating and oxidation treatment in catalytic converter technology.



### 1.3 Hypothesis

The ultrasonic technique via cavitation bubbles and high velocity can make the surface deformation and also can accelerate the  $\gamma\text{-Al}_2\text{O}_3$  powders, so that it can bombardment to the Fe-Cr-Al surface. These collisions generate sufficient heat and  $\gamma\text{-Al}_2\text{O}_3$  layer can form on the Fe-Cr-Al surface. Electroplating process in addition is to embed the nickel and strengthen the adhesion when oxidized. The expected outcomes are the layer of  $\gamma\text{-Al}_2\text{O}_3$  and nickel will embed on the Fe-Cr-Al metallic substrates. The combination of oxide of  $\gamma\text{-Al}_2\text{O}_3$  and NiO can be able to grow and provide oxidation resistance on coated Fe-Cr-Al in long-term oxidation in range of 500, 700, 900 and 1100 °C for 100 hours. The utilization of  $\gamma\text{-Al}_2\text{O}_3$  as a washcoat onto Fe-Cr-Al support needs a comprehensive study for catalytic converter, which works in high temperature condition between 900 and 1100 °C on the close-coupled catalytic converter and under-floor catalytic converter at temperature between 500 and 700 °C.

### 1.4 Aim of study

The aim of this research is to develop  $\gamma\text{-Al}_2\text{O}_3$  washcoat on Fe-Cr-Al substrate by ultrasonic treatment combined with nickel electroplating and oxidation treatment for catalytic converter application

### 1.5 Objective of study

- i. To develop  $\gamma\text{-Al}_2\text{O}_3$  washcoat on Fe-Cr-Al metallic substrates for catalytic converter application.
- ii. To identify the oxide phase of  $\text{Al}_2\text{O}_3$  on coated Fe-Cr-Al after oxidation.
- iii. To enhance the oxidation resistance of coated Fe-Cr-Al in long-term high temperature oxidation.
- iv. To produce  $\gamma\text{-Al}_2\text{O}_3$  layer as a washcoat for catalytic converter application.

## 1.6 Scope of study

The scopes of this research as follows:

- i. Effect of ultrasonic treatment on  $\gamma$ -Al<sub>2</sub>O<sub>3</sub> powder in particle size distributions.
- ii. Study the effect of  $\gamma$ -Al<sub>2</sub>O<sub>3</sub> on Fe-Cr-Al substrate after ultrasonic treatment.
- iii. Study of nickel electroplating methods in order to obtain deposition technique of nickel on the Fe-Cr-Al metallic monolith.
- iv. Long-term oxidation between 500 and 700 °C of coated Fe-Cr-Al substrate to simulate under-floor catalytic condition.
- v. Long-term oxidation between 900 and 1100 °C of coated Fe-Cr-Al substrate to simulate close-coupled catalytic converter which works in high temperature condition.
- vi. The relationship between weight gain and oxidation period.
- vii. Study the parabolic rate constant ( $k_p$ ) of the kinetics oxidation.
- viii. Phase analysis of coated Fe-Cr-Al after long term oxidation.
- ix. Material characterization using Scanning Electron Microscopy (SEM) attached with Energy Dispersive X-ray Spectroscopy (EDS) and X-ray Diffraction (XRD).

## CHAPTER 2

### LITERATURE REVIEW

The literature review focused on catalytic parameters of close-coupled and under-floor converter application, the fundamental of catalyst materials aspects, washcoat,  $\text{Al}_2\text{O}_3$  as a washcoat and development, ultrasonic, electroplating, oxidation behavior related to catalytic converter parameters will discussed in this section.

#### 2.1 Catalytic converter

Catalytic converter is a device that located in-line with the exhaust system and is used to cause a desirable chemical reaction to take place in the exhaust flow (George, 2006). Close-coupled converters, also called light-off converters, mount on or near the engine manifold. They can provide the first step in removal of gaseous pollutants such as hydrocarbons (HC), whereas the under-floor catalyst removed the remaining carbon monoxide (CO) and nitrogen oxides ( $\text{NO}_x$ ) (Heck *et al.*, 2009).

The use of a Three-Way Catalytic (TWC) converter that was constructed of catalyst coated pellets tightly packed in a sealed shell, while later model vehicles are equipped with a monolith type TWC that uses a honeycomb shaped catalyst element. While both types operate similarly, the monolith design creates less exhaust backpressure, while providing ample surface area to efficiently convert feed gases. As engine exhaust gases flow through the converter passageways, they contact the coated surfaces which initiate the catalytic process. When exhaust and catalyst temperatures rise, the following reaction occurs, oxides of nitrogen ( $\text{NO}_x$ ) are reduced into simple nitrogen ( $\text{N}_2$ ) and carbon dioxide ( $\text{CO}_2$ ). Hydrocarbons (HC) and

carbon monoxides (CO) are oxidized to create water (H<sub>2</sub>O) and carbon dioxide (CO<sub>2</sub>) (Fahrul, 2010).

A catalytic converter consists of a several component such as substrate, washcoat and catalyst material through which hot exhaust gas must pass before being discharged into the air as shown in Figure 2.1.

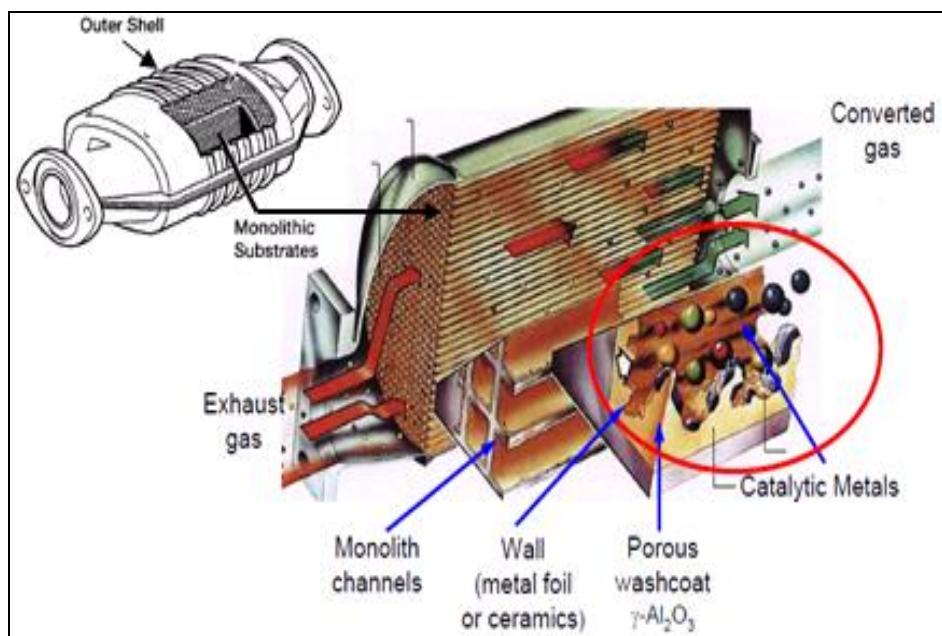


Figure 2.1: Structure of catalytic converter (Harkonen, 2005)

The performance-based catalytic converter reengineering effort has had three main focuses: (1) wide application of close-coupled converters mounted near the exhaust manifold of engines for improved performance following a cold engine start; (2) the development of thin-wall, high-cell-density substrates for improved contacting efficiency between the exhaust gas and the active catalyst, and lowering the thermal mass of the converter; (3) the design of advanced, high-performance TWCs for both close-coupled and under-floor converter applications that emphasize excellent thermal durability (Kubsh, 2006). Figure 2.2 shows the parameters affecting on the catalyst performance.

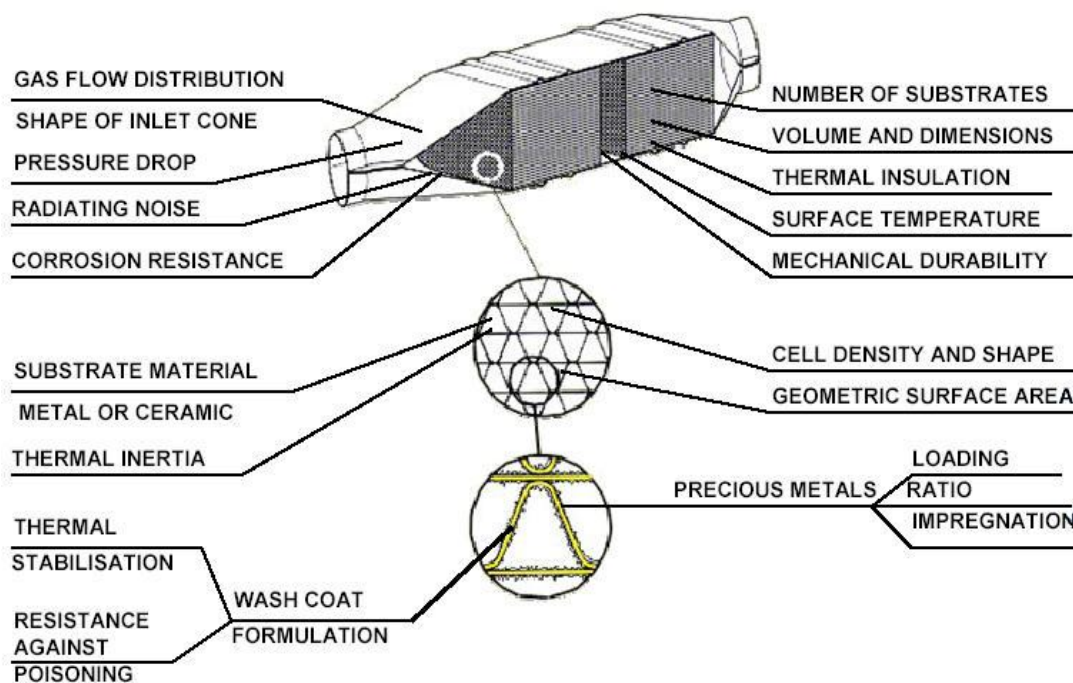


Figure 2.2: Parameters affecting on the catalyst performance (Harkonen, 2005)

### 2.1.1 Substrate

A substrate is a substance on which some other substance is absorbed or in which it is absorbed. The two most common products available in the market are ceramic and metallic substrates. Both substrates have relatively low porosity that makes them unsuitable as a catalyst support. To overcome this, a thin layer of a porous material is applied to the channel walls. This thickness layer typically about 20-150  $\mu\text{m}$  is referred to as washcoat (Santos & Costa, 2008). The substrate typically provides a large number of parallel flow channels to allow for sufficient contacting area between the exhaust gas and the active catalytic materials without creating excess pressure losses (Kubsh, 2006).

The application of ceramic and metal substrate technology has contributed a major benefit in catalytic converter technology. A larger catalyst surface area can be incorporated into a given converter volume and this allows better conversion efficiency and durability. The thin walls reduce thermal capacity and avoid the penalty of increased pressure losses. Alternatively the same performance can be

incorporated into a smaller converter volume, making the catalyst easier to fit close to the engine, as cars get more compact (Bode, 1997).

Currently, different cell shapes are commonly used in both metal and ceramic substrates: sinusoidal, triangular, square and hexagonal (Heck *et al.*, 2001). The geometrical surface area (GSA) of the catalytic converter substrate is determined by the cell density, cell shape and converter volume. The rate of conversion in warmed-up condition is limited by the rate of the mass transfer from the channel to the catalytic wall. The mass transfer in a smooth channel represents a process of diffusion and is thus accelerated by a rise in temperature and the difference of pollutants concentration radially. As the concentration of pollutant substances in the converter channels decreases because of already converted pollutants the difference in concentration between the channel core and wall as a driving force becomes increasingly lower (Bode, 1997).

#### **2.1.1.1 Metallic substrate**

Metal-foil-based substrates are made from ferritic-based stainless steel foils brazed together to form the parallel flow passages. The ferritic foil alloy provides good oxidation resistance in the exhaust environment, good mechanical strength, and an oxidized surface that promotes good adhesion of the catalytic coating to the foil (Kubsh, 2006). Ferritic steels became available that could be made into ultra thin foils, corrugated and then laid up to form a honeycomb structure. In the beginning the foils could be made from material only 0.05 mm thick allowing high cell densities to be achieved. Complex internal structures can be developed and today wall thickness is down to 0.025 mm and cell densities of 800, 1000 and 1200 cpsi are available (Bode, 1997).

Metal wire has been attempts to utilize wire meshes made of cheap iron or stainless steel as support of active catalyst component. However, there have low surface areas. The wire surface is usually coated with a refractory material of inorganic powder since catalytically active metals or metal oxides can be well dispersed by such a modified surface of wire mesh (Yang *et al.*, 2003).

Monoliths made of stainless steel or steel alloys are becoming increasingly popular as catalyst-supports, mainly because they can be prepared with thinner walls which offer the potential for higher cell densities with lower pressure drop and with higher thermal conductivity, resulting in faster heat-up comparing with the ceramic supports. However, the common designs of steel monoliths, such as corrugated sheets and plain sheets welded or wrapped together into a monolithic structure, may reduce inter-phase mass/heat transfer rates and suppress radial mixing (Sun *et al.*, 2007).

Metallic monoliths became available in the early 1990s. Because of their high open frontal areas, approaching 90 %, the metallic monoliths provide higher geometric surface area while offering lower resistance to flow, i.e. back pressure. Furthermore, metallic monoliths are being used extensively in close coupled applications due to their higher thermal conductivity that guarantees more uniform temperature distribution between the monolith channels as compared to that of ceramic monoliths. The metallic substrate presents better conversions, particularly for HC and CO at high space velocities as compared to the ceramic substrate, mainly because of its larger geometric surface area and lower transverse pecelet number (Santos & Costa, 2008). The metallic monolith substrate is shown in Figure 2.3.

Fe-Cr-Al metallic monoliths present some advantages over cordierite ceramic monoliths such as higher thermal conductivity, lower heat capacities, greater thermal and mechanical shock resistance (Zeng *et al.*, 2007). Fe-Cr-Al also easy manufactured as honeycomb substrate with thinner walls, a lower pressure drop and higher contact surface area (Wu *et al.*, 2005). The corrugated and spiral shaped tools have been successfully designed and developed for manufacturing the hand-made catalytic converter in full scale size using Fe-Cr-Al foil as the catalytic substrate monolith (Fahrul *et al.*, 2009).



Figure 2.3: The design of metallic monolith substrate (VBulletin Solutions Inc, 2011)

### 2.1.1.2 Fe-Cr-Al metallic substrate

Fe-Cr-Al alloys are often used in high temperature applications like support material for catalytic converters, heating elements in furnaces, burner elements and hot gas filters. When exposed to high temperatures an alumina film grows on the surface of the Fe-Cr-Al material. In order to provide a good protection the alumina should grow slowly, be adherent, dense and inert, which is true for  $\alpha$ -Al<sub>2</sub>O<sub>3</sub>. Besides the only stable form  $\alpha$ -Al<sub>2</sub>O<sub>3</sub>, alumina has several metastable polymorphs such as  $\gamma$ -,  $\theta$ - and  $\delta$ -Al<sub>2</sub>O<sub>3</sub>, which provides less protection in corrosive environments.

In practice the amount of Al in the alloy is limited to about 7 wt.%, by the fact that higher concentrations of Al make the alloy brittle and impossible to process by conventional rolling. Thin foil Fe-Cr-Al materials are more sensitive to Al depletion during oxidation due to a minor total Al reservoir than in bulk Fe-Cr-Al materials. Fe-Cr-Al materials are usually alloyed with reactive elements (RE) such as zirconium (Zr), yttrium (Y), cerium (Ce), lanthanum (La) or hafnium (Hf). Although the exact effects of reactive elements on the oxidation characteristics are not known, reactive elements may influence the oxide growth mechanism and improve the oxide scale adhesion (Engkvist *et al.*, 2009).



The corrosion resistance of Fe-Cr-Al in oxidizing atmosphere is due to the formation of a highly protective chromium and aluminum oxide layer on the surface, which effectively separates the oxidizing atmosphere from the pure alloy. Because  $\alpha$ -Al<sub>2</sub>O<sub>3</sub> is very stable at high temperatures it would be beneficial to maximize its content at the surface (Airiskallio *et al.*, 2010).

## 2.2 Washcoat

The honeycomb ceramic support is coated with a material of high surface area called the washcoat, which acts as a host for the noble metal catalysts. The most widely used material in the application of washcoat is Al<sub>2</sub>O<sub>3</sub>, especially for environmental applications (Agrafiotis & Tsetsekou, 2000). At one time it was thought to provide only a surface to disperse the catalytic substance to maximize the catalytic surface area as illustrated in Figure 2.4. However, it is now clear that it can play a critical role in maintaining the activity, selectivity and durability of the finished catalyst.

Generally, the most common carriers are the high surface area inorganic oxides, most of which is Al<sub>2</sub>O<sub>3</sub>. The pollutant containing gases enter the channels uniformly and diffuse to and through the washcoat pore structure to the catalytic sites where they are converted catalytically. The amount of geometric surface area, upon which the washcoat is deposited, is determined by the number and diameter of the channels. There is a limit as to how much washcoat can be deposited, since too much result in a decrease of the effective channel diameter, thereby increasing the pressure drop to an unacceptable level.  $\gamma$ -Al<sub>2</sub>O<sub>3</sub> have large surface area, good pore size distribution, surface acidic properties, composition of trace components and crystal structure (Heck *et al.*, 2009).

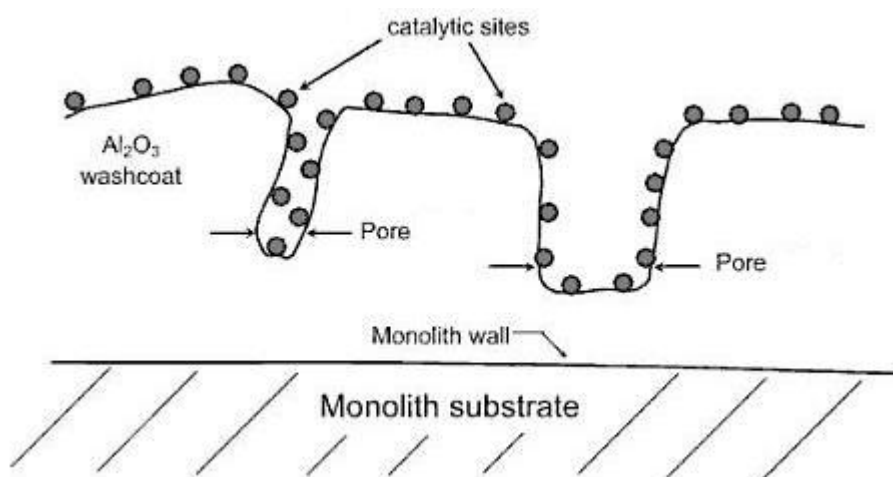


Figure 2.4: Schematic diagram for catalytic sites dispersed on a high surface area of  $\text{Al}_2\text{O}_3$  carrier bonded to a monolith support (Heck *et al.*, 2009)

### 2.2.1 $\text{Al}_2\text{O}_3$ washcoat

$\text{Al}_2\text{O}_3$  is the most commonly material oxide used as carrier/washcoat in environment catalysis technology. It will be used to develop a model of a heterogeneous catalyst. To maximize reaction rates, it is essential to ensure the accessibility of all reactants to the active catalytic component sites dispersed within the internal pore network of the washcoat. Many different sources of alumina have various surface characterization including areas, pore size distributions, surface acidic properties, composition of trace components and crystal structures. Its chemical and physical properties depend on sample preparation, purity and thermal history. An image of  $\gamma\text{-Al}_2\text{O}_3$  and  $\alpha\text{-Al}_2\text{O}_3$  for scanning electron micrograph analysis at 80.000 magnifications is shown in Figure 2.5.  $\gamma\text{-Al}_2\text{O}_3$  have a surface area of about  $150 \text{ m}^2/\text{g}$ . It is clearly seen that the structure composed of primary  $\text{Al}_2\text{O}_3$  particles agglomerated forming highly porous networks (Heck *et al.*, 2009).

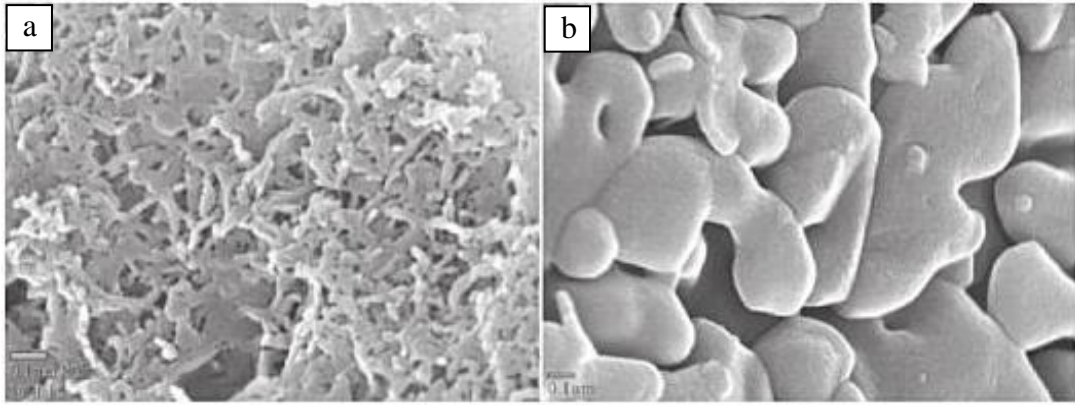


Figure 2.5: (a) Scanning electron microscope (SEM) image of gamma ( $\gamma$ - $\text{Al}_2\text{O}_3$ ), (b) SEM of alpha ( $\alpha$ - $\text{Al}_2\text{O}_3$ ) (Heck *et al.*, 2009)

Oxidations of  $\text{Al}_2\text{O}_3$  have a several of phases at different temperatures including (eta)  $\eta$ - $\text{Al}_2\text{O}_3$  (300-800 °C), (gamma)  $\gamma$ - $\text{Al}_2\text{O}_3$  (500-800 °C), (delta)  $\delta$ - $\text{Al}_2\text{O}_3$  (800-1000 °C), (theta)  $\theta$ - $\text{Al}_2\text{O}_3$  (1000-1100 °C) and (alpha)  $\alpha$ - $\text{Al}_2\text{O}_3$  (>1100 °C).

At roughly 500 °C, it converts to  $\gamma$ - $\text{Al}_2\text{O}_3$ , which typically has an internal surface area of 100-200  $\text{m}^2/\text{g}$ . Continuous heating causes additional sintering and/or phase changes and loss of surface hydroxyl ( $\text{OH}^-$ ) groups up to about 1100 °C, where it converts to the lowest internal surface area structure (1-5  $\text{m}^2/\text{g}$ ). This is called  $\alpha$ - $\text{Al}_2\text{O}_3$ . SEM image in Figure 2.5b clearly shows that its morphology is much more densely packed than the  $\gamma$ - $\text{Al}_2\text{O}_3$  shown in Figure 2.5a. This transformation is due to time-temperature relationships and also depends on the exposure environment.

Transition phases of aluminum oxide such as the  $\gamma$ -phase and the amorphous phase are mainly produced at temperatures below 950 °C as well as different morphologies and grain sizes can be obtained (Nable *et al.*, 2003). Thermal oxidation have revealed that the scale might contain  $\alpha$ - $\text{Al}_2\text{O}_3$  with a small amount of a  $\theta$ - $\text{Al}_2\text{O}_3$  phase, which afterwards transforms into an  $\alpha$ - $\text{Al}_2\text{O}_3$  or  $\gamma$ - $\text{Al}_2\text{O}_3$  phase depending on the temperature and the density of the oxidizing atmosphere over the steel surface (Reszka *et al.*, 2006).

### 2.3 Particle size distribution of the carrier / washcoat

The particles in a colloidal suspension or emulsion are seldom with the same size but varying in shapes. The size and shape is therefore a significant problem. Emulsion droplets can usually be assumed to be spherical (long as the distance between the droplets is large enough). For solid particles general descriptions of shape like spheroidal, rod- or disk-shaped, even when the system contains individual particles with other shapes. The particle size may also vary over quite a wide range. It is not unusual for the particles of a suspension produced in a grinding operation, for example, to vary by a factor of 100 from the smallest to the largest size. To describe such situations, it normally breaks the range up into a number of classes and try to find out how many particles are in each size range. This range is called the particle size distribution (PSD), and it can be represented in the form of a histogram (Figure 2.6) (Heck *et al.*, 2009).

The size of the agglomerated particles that make up the carrier must be compatible with the surface roughness and macro-pore structure of the carrier powders to produce the uniform particle size which will be coated on substrate. Sieves of various mesh sizes have been standardized, and thus, one can determine particle size ranges by noting the percentage of material, usually based on weight, that passes through one mesh size but is retained on the next finer screen based on standard ASTM D4513-85, (1998). The stack of sieves is vibrated, allowing the finer particles to pass through coarser screens until retained by those screens finer in opening than the particle size of the material of interest. Each fraction is then weighed and a distribution is determined.

This method is reliable only for particles larger than about 40 micron. Below this size, sieving is slow and charging effects influence measured values. Sophisticated instrumentation is available for measuring the distribution of finer  $\text{Al}_2\text{O}_3$  particles. Recently, particle size analyzer (PSA) has been found effective. An example of particles size analyzer and distribution for an  $\text{Al}_2\text{O}_3$  carrier using CILAS is illustrated in Figure 2.6. The values on the left of Y-axis indicate the cumulative % of particles, the size of which is displayed on the highest peak of X-axis. The right axis shows the % distribution for a given particle size (Heck *et al.*, 2009). There are two types of graph which each of them represents particle size distribution and cumulative particle size. The median size (which in this case corresponds to the

maximum frequency) and the spread of the particles distribution is represented by the maximum peak.

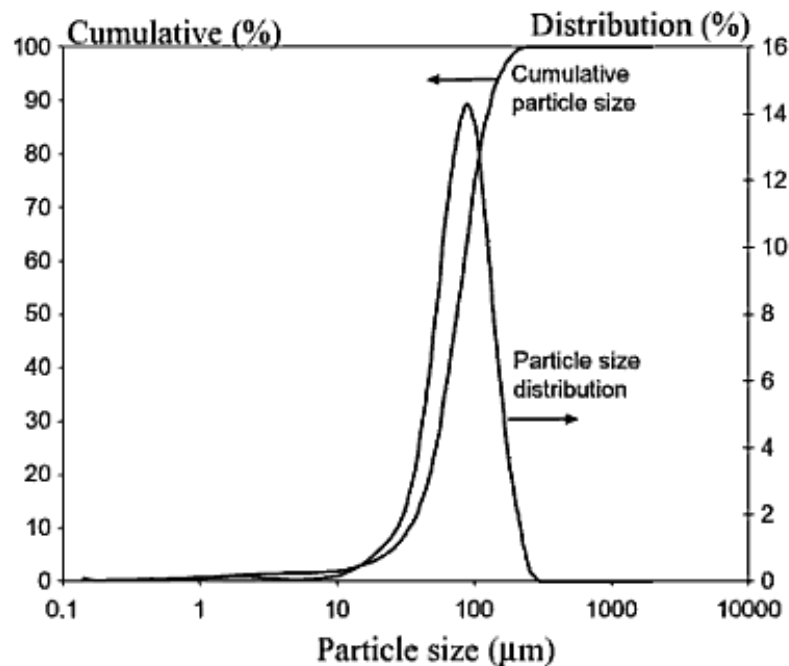


Figure 2.6: Particle size measurement using CILAS particle size analyzer (PSA) (Heck *et al.*, 2009)

#### 2.4 Washcoat development on Fe-Cr-Al metallic substrate

In addition to the microstructural requirements for a washcoat material, excellent adhesion on the substrate is a further crucial requirement and optimization of the parameters that affect the adhesion of the washcoat layer on the support is imperative. Reduction of the washcoat powder size (less than 2 microns) down to colloidal dimensions seems to be necessary for the achievement of satisfactory adhesion and endurance of the washcoat under the severe operating conditions (Agrafiotis & Tsetsekou, 2000).

For the washcoat, the higher surface area is very desirable (Jiang *et al.*, 2005). Besides the surface area, other desirable washcoat properties are thermal stability and appropriate pore size distribution. A material combining these properties and most widely used in washcoat application is  $\gamma$ -Al<sub>2</sub>O<sub>3</sub>. The washcoat phase usually

contains smaller quantities of other phases, which have a particular function. For example, cerium (Ce) and lanthanum (La) are frequently added to  $\gamma$ -Al<sub>2</sub>O<sub>3</sub> in order to induce oxygen storage capacity and thermal stability respectively (Agrafiotis & Tsetsekou, 2000).

The main problem for the washcoat is to maintain a high geometric surface area, appropriate pore size distribution and firm cohesion to the support at high temperatures (Wu *et al.*, 2001). The coating adhesion between the metallic support and the ceramic washcoat becomes a problem. The deposition of the  $\gamma$ -Al<sub>2</sub>O<sub>3</sub> washcoat on the metallic monolith has not been as well developed yet as that on the ceramic monolith. The non-porous nature of the metal foil, coupled with the mismatch in the thermal expansion between the foil and the ceramic washcoat, contributes to a washcoat adhesion problem during thermal cycling (Wu *et al.*, 2005).

The utilization of Al<sub>2</sub>O<sub>3</sub> as catalyst combined with Fe-Cr-Al as a support needs a comprehensive study due to its chemical and physical changing at catalytic converter. For example, the coating adhesion between the metallic support and the ceramic washcoat becomes a problem due to it has different thermal expansion coefficients. In previous investigation, washcoat development was deposited by sol-pyrolysis method (Zheng *et al.*, 2007), precipitation and dip-coating method (Valentini *et al.* (2001), impregnation method (Betta, 1997), plasma spraying technique (Wu *et al.*, 2001), situ hydrothermal method (Wei *et al.*, 2005) and electrophoretic deposition (Sun *et al.*, 2007). These methods must be conducted through a complicated sequence to obtain the washcoat requirements. Therefore, this research will discuss the ultrasonic treatment with nickel electroplating combine with oxidation for developing  $\gamma$ -Al<sub>2</sub>O<sub>3</sub> washcoat on Fe-Cr-Al substrate. This method is simple and cheaper than previous research.

## 2.5 Catalyst materials for catalytic converter

The use of catalyst material is to stimulate or enhance a chemical reaction that naturalize or reduce the toxic by-products of combustion. As exhaust and catalyst temperatures rise, the following reaction occurs, oxides of nitrogen ( $\text{NO}_x$ ) are converted into simple nitrogen ( $\text{N}_2$ ) and carbon dioxide ( $\text{CO}_2$ ). Hydrocarbons (HC) and carbon monoxides (CO) are oxidized to create water ( $\text{H}_2\text{O}$ ) and carbon dioxide ( $\text{CO}_2$ ). In automobiles, this typically results in 90% conversion of carbon monoxide, hydrocarbons, and nitrogen oxides into less concentration gas which leads to environmental friendly. Catalysts are either platinum-group metals or base metals such as chromium, nickel, and copper which are heated by exhaust gas in range of 500 - 700 °C. At this temperature unburned hydrocarbons and carbon monoxide are further oxidized, while oxides of nitrogen are chemically reduced in a second chamber with a different catalyst. Platinum-group metals or noble metals are any of several metallic chemical elements that have outstanding resistance to oxidation, even at high temperatures. The noble metals that used as a catalyst material is usually include rhenium, ruthenium, rhodium, palladium, silver, osmium, iridium, platinum, and gold. However, these materials are limited supply sources and expensive (George, 2006).

### 2.5.1 Nickel as catalyst material

The catalytic properties, metal dispersion and the structural features of species depend on the method to process these materials and on the support used. The usage of catalyst will depend on the type of dopant used in order to form a durable, sulfur tolerant, high catalytic activity catalyst. In many cases, the selected dopants studied were magnesium (Mg), zirconium (Zr), molybdenum (Mo), manganese (Mn), ferum (Fe), cobalt (Co) and copper (Cu) (Valentini *et al.*, 2003).

The Ni-based catalysts have high activity, stability and selectivity. Therefore, the development of such catalysts is an attractive challenge (Valentini *et al.*, 2004). The investigation of a Ni-based steam reforming catalyst was developed for the coating of microstructures (Stefanescu *et al.*, 2007).

Nickel oxide (NiO) exhibited high activity and selectivity of methane due to the ability of NiO to undergo reduction process owing to the presence of defect sites of the surface. Despite of the fast catalyst deactivation and carbon deposition, NiO catalyst was favorable due to its high thermal stability and low price. Therefore, nickel oxide can be considered as the best catalyst material for catalytic converter (Buang *et al.*, 2008).

The catalysts for catalytic converter are mostly related to the precious group of metals platinum (Pt), palladium (Pd) and rhodium (Rh) (Kirby, 2009). However these materials are expensive, therefore some materials are used as a substitute such as nickel. Nickel oxide (NiO) catalyst could be a potential candidate in catalyst material and cheaper than precious group of metals platinum (Pt), palladium (Pd) and rhodium (Rh). Nickel oxide application is also effectively for the NO<sub>x</sub> absorber catalyst in order to reduce the emissions of hydrogen sulfide (H<sub>2</sub>S) during desulfation (Elwart, 2006). The utilization of nickel as catalyst combined with Fe-Cr-Al as a support needs a comprehensive study due to catalytic converter which works in high temperature condition (Dou, 2005). NiO produced from a heated pure nickel at 900 °C that the oxide grain size is sufficiently large for lattice diffusion to predominate over grain boundary transport (Young, 2008).

## **2.6 Ultrasonic surface treatment**

Surface deformation is a widespread and effective method for hardening metallic materials. With this method, the surface of a material properties can be improved is a subject of high compressive stresses, which results in a better product strength, durability, and reliability. Many surface deformation techniques have been employed including rolling, ball treatment, and shot blasting (peening). Ultrasonic surface hardening provides an efficient alternative because it can reduce the time. Applied ultrasonic vibrations relieve residual stresses and improve surface finish and hardness, thereby providing a better wear resistance of products (Mason & Lorimer, 2002).



Recently an ultrasonic surface treatment, similar to shot peening, has been developed. In this process a powerful ultrasonic field is generated to transfer high kinetic energy to steel balls that hit the surface of the workpiece being treated. The energy transferred to the workpiece during a one-ball impingement event is small. The required surface strain is achieved through repeated action on the surface of the workpiece. The process creates homogeneous residual stress simultaneously on each side of the parts to be treated. The process will act on improvement of the surface of the material.

### **2.6.1 Reactions involving metal or solid surfaces**

There are two types of chemical reaction occurred on the material surface, first in which the metal is a reagent and is consumed in the process and second in which the metal functions as a catalyst. While it is certainly true that any cleaning of metallic surfaces will enhance their chemical reactivity, in many cases it would seem that this effect alone is not sufficient to explain the extent of the sonochemically enhanced reactivity. In such cases it is thought that sonication method serves to sweep reactive products, clear of the metal surface and thus present renewed clean surfaces for reaction. Other methods include the possibility of enhanced single electron transfer (SET) reactions at the surface (Mason & Lorimer, 2002).

### **2.6.2 Reactions involving powders or other particulate matter**

Just as with the metal surface reactions described above, the efficiency of heterogeneous reactions involving solids dispersed in liquids will depend upon the available reactive surface area and mass transfer. Conventional technology involves agitating and stirring with rotating devices and baffled pipes as the processors of fluids when mixing, reacting or dissolving small and submicron sized particles on an industrial scale. This can take many hours, days or even weeks until the desired properties are obtained. The main problem with conventional rotational mixing

techniques, when trying to disperse solid particles of 10 microns in diameter or smaller in a liquid is that the rate of mixing and mass transfer of these particles through the medium reaches a maximum. In fact the mass transfer coefficient  $K$  reaches a constant value of about  $0.015 \text{ cm s}^{-1}$  in water, and speed of rotational agitation, no matter how large this increase may be. Sonication provides a solution to this problem in that power ultrasound will give greatly enhanced mixing (Mason & Lorimer, 2002).

## 2.7 Acoustic cavitation

Power ultrasound enhances chemical and physical changes in a liquid medium through the generation and subsequent destruction of cavitation bubbles. Like any sound wave ultrasound is propagated via a series of compression and rarefaction waves induced in the molecules of the medium through which it passes (Suslick, 2000). At sufficiently high power the rarefaction cycle may exceed the attractive forces of the molecules of the liquid and cavitation bubbles will form. Such bubbles grow by a process known as rectified diffusion i.e. small amounts of vapour (or gas) from the medium enters the bubble during its expansion phase and is not fully expelled during compression. The bubbles grow over the period of a few cycles to an equilibrium size for the particular frequency applied. It is the fate of these bubbles when they collapse in succeeding compression cycles which generates the energy for chemical and mechanical effects (Figure 2.7). Cavitation bubble collapse is a remarkable phenomenon induced throughout the liquid by the power of sound. In aqueous systems at an ultrasonic frequency of 20 kHz each cavitation bubble collapse acts as a localised "hotspot" generating temperatures of about 4,000 K and pressures in excess of 1000 atmospheres.

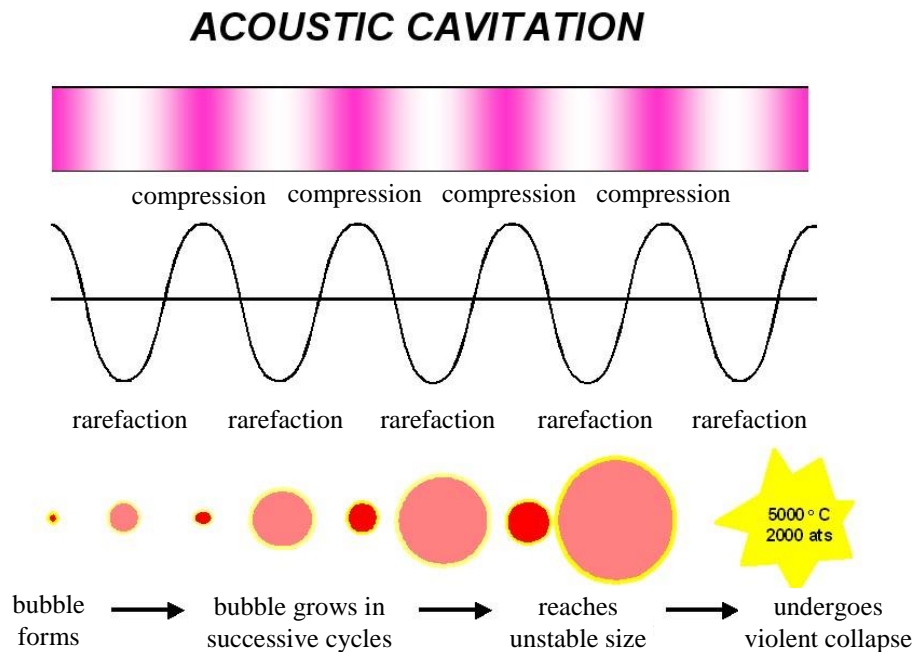


Figure 2.7: Generation of an acoustic bubble (Suslick, 2000)

The cavitation bubble has a variety of effects within the liquid medium depending upon the type of system in which it is generated. These systems can be broadly divided into homogeneous liquid, heterogeneous solid/liquid and heterogeneous liquid/liquid. Within chemical systems these three groupings represent most processing situations (Suslick, 2000).

### 2.7.1 Cavitation near a surface

Unlike cavitation bubble collapse in the bulk liquid, collapse of a cavitation bubble on or near to a surface is unsymmetrical because the surface provides resistance to liquid flow from that side. The result is an inrush of liquid predominantly from the side of the bubble remote from the surface resulting in a powerful liquid jet being formed, targeted at the surface (Figure 2.8). The effect is equivalent to high pressure jetting and is the reason that ultrasound is used for cleaning. This effect can also activate solid catalysts and increase mass and heat transfer to the surface by disruption of the interfacial boundary layers.

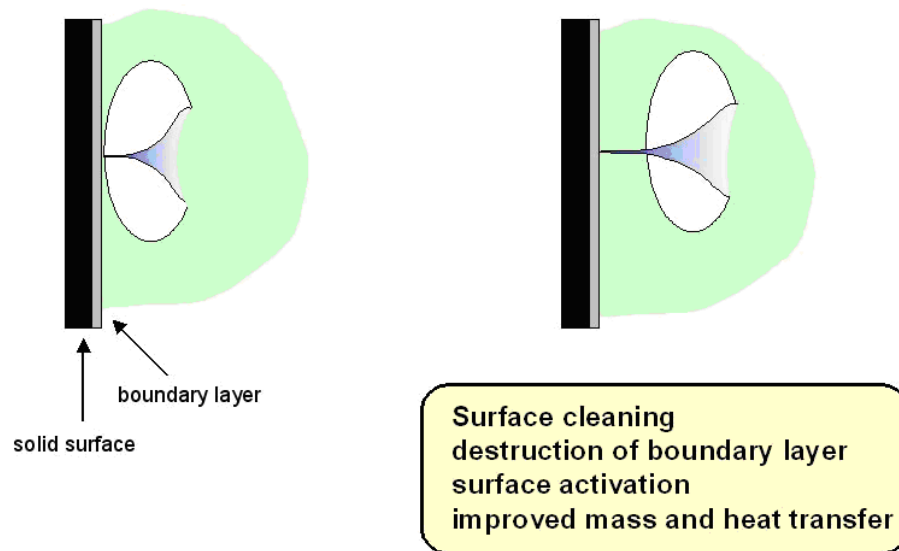


Figure 2.8: Cavitation bubble collapse at or near a solid surface (Suslick, 2000)

### 2.7.2 Heterogeneous powder-liquid reactions

Acoustic cavitation can produce dramatic effects on powders suspended in a liquid (Figure 2.9). Surface imperfections or trapped gas can act as the nuclei for cavitation bubble formation on the surface of a particle and subsequent surface collapse can then lead to shock waves which break the particle apart. Cavitation bubble collapse in the liquid phase near to a particle can force it into rapid motion. Under these circumstances the general dispersive effect is accompanied by interparticle collisions which can lead to erosion, surface cleaning and wetting of the particles and particle size reduction (Suslick, 2000).

## ACOUSTIC CAVITATION *In the presence of a suspended powder*

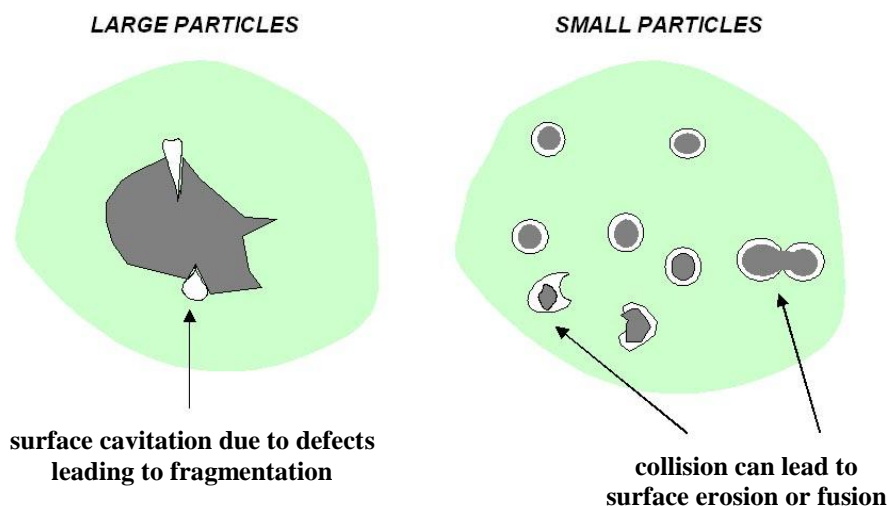


Figure 2.9: Acoustic cavitation in a liquid with a suspended powder (Suslick, 2000)

In heterogeneous liquid/liquid reactions, cavitation collapse at the interface will cause disruption and mixing, resulting in the formation of very fine emulsions (Figure 2.10).

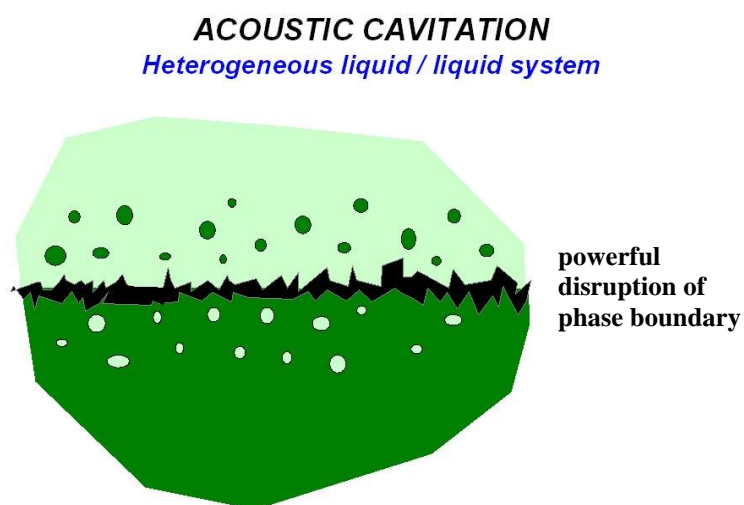


Figure 2.10: Cavitation effects in a heterogeneous liquid system (Suslick, 2000)

## REFERENCES

- Agrafiotis, C. & Tsetsekou, A. (2000). The effect of powder characteristics on washcoat quality. Part I: Alumina washcoats. *European Ceramic Society*, 20, pp. 815-824.
- Airiskallio, E., Nurmi, E., Heinonen, M. H., Vayrynen, I. J., Kokko, K., Ropo, M., Punkkinen, M. P. J., Pitkanen, H., Alatalo, M., Kollar, J., Johansson, B. & Vitos, L. (2010). High temperature oxidation of Fe-Al and Fe-Cr-Al alloys: The role of Cr as a chemically active element. *Corrosion Science*, 52, pp. 3394-3404.
- Badini, C. & Laurella, F. (2001). Oxidation of FeCrAl alloy: influence of temperature and atmosphere on scale growth rate and mechanism. *Surface & Coatings Technology*, 135, pp. 291-298.
- Betta, D. (1997). *Introduction to Catalytic Combustion*. Amsterdam. Amsterdam: Gordon & Breach Science Publishers.
- Birks, N., Meier, G. H. & Pettit, F. S. (2006). *Introduction to the High-Temperature Oxidation of Metal*. 2<sup>nd</sup> ed. USA: Cambridge University Press.
- Bode, H. (Ed.) (1997). *Metal-Supported Automotive Catalytic Converters*. Germany: Werkstoff-Informationsgesellschaft mbH.
- Bode, H. (Ed) (2002). *Materials Aspects in Automotive Catalytic Converters*. Germany: WILEY-VCH Verlag GmbH.

- Brylewski, T., Dabek, J. & Przybylski, K. (2004). Oxidation kinetics study of the iron-based steel for solid oxide fuel cell application. *Thermal Analysis and Calorimetry*, 77, pp. 207-216.
- Buang, N. A., Bakar, W. A. W. A., Marsin, F. M. & Razali, M. H. (2008). CO<sub>2</sub> / H<sub>2</sub> methanation on nickel oxide based catalyst doped with various elements for the purification of natural gas. *The Malaysian Journal of Analytical Sciences*, 12, pp. 217-223.
- Cilas Particle Size Analyzer. (2004). *Frequently Asked Questions on Particle Size Analyse by Laser Diffraction*. (France): Cilas Tutorials.
- Colloidal Dynamics Pty Ltd. (1999). *Particle Size Distributions*. Eveleigh (Australia): Electroacoustics Tutorials.
- Connolly, J. R. (2007). *Elementary crystallography for X-ray diffraction*. Spring, pp. 1-13.
- Dou, D. (2005). *NiO Catalyst Configurations, Methods for Making NO<sub>x</sub> Absorbers, and Methods for Reducing Emissions*. U.S. Patent 6,930,073 B2.
- Elwart, S. (2006). *Sistem and Method for Removing Hydrogen Sulfide from an Emissions Stream*. U.S. Patent 7,104,045 B2.
- Engkvist, J., Grehk, T. M., Bexell, U. & Olsson, M. (2009). Early stages of oxidation of uncoated and PVD SiO<sub>2</sub> coated FeCrAl foils. *Surface & Coatings Technology*, 203, pp. 2845-2850.
- Fahrul, M. (2010). *Development and Application of a Computer Aided Engineering Methodology Supporting the Design Optimization of Automotive Exhaust Treatment System*. Universiti Tun Hussein Onn Malaysia: Master Thesis.

- Fahrul, M., Sebayang, D. & Untoro, P. (2009). Apparatus for Producing a Spiral Shape of Corrugated Sheet Metal for Catalyst Substrate of Catalytic Converter. *Proc. Of Int. Conf. on Advances in Mechanical Engineering*.
- George, D. B. (1994). *Nickel Plating*. 5<sup>th</sup> ed. USA: ASM International.
- George, S. (2006). *The Catalytic Converter*. Retrieved Oct 20, 2010.
- Ghosh, J., Mazumdar, S., Das, M., Ghatak, S. & Basu, A.K. (2008). Microstructural characterization of amorphous and nanocrystalline boron nitride prepared by high energy ball milling. *Materials Research Bulletin*, 43, pp. 1023-1031.
- Harkonen, M. (2005). *Exhaust Gas Catalysts*. Nanotechnology in Northern Europe Helsinki Fair Center. Ecocat Oy.
- Haugrud, R. (2003). On the high temperature oxidation of nickel. *Corrosion Science*, 45, pp. 211-235.
- Heck, R.M., Farrauto, R.J. & Gulati, S.T. (2009). *Catalytic Air Pollution Control Commercial Technology*. 3<sup>rd</sup> ed. USA: John Wiley & Sons, Inc.
- Jiang, P., Lu, G., Guo, Y., Guo, Y., Zhang, S. & Wang, X. (2005). Preparation and properties of a  $\gamma$ -Al<sub>2</sub>O<sub>3</sub> washcoat deposited on a ceramic honeycomb. *Surface & Coatings Technology*, 190, pp. 314-320.
- Kirby, C. W. (2009). *Catalytic Converter having Three Precious Catalyst Materials*. European Patent Application 734,757 A1.
- Kubsh, J. (Ed.) (2006). *Advanced Three-way Catalysts*. USA: Society of Automotive Engineers.
- Lee, D., Santella, M. L., Anderson, I. M. & Pharr, G. M. (2005). Long-term oxidation of an as-cast Ni<sub>3</sub>Al alloy at 900 oC and 1100 oC. *Metallurgical and Materials Transactions*, 36 A, pp. 1855-1869.



- Mason, T. J. & Lorimer, J. P. (2002). *Applied Sonochemistry: Uses of Power Ultrasound in Chemistry and Processing*. Weinheim: Wiley-VCH Verlag GmbH.
- Nable, J., Gulbinska, M., Suib, S. L. & Galasso, F. (2003). Aluminum oxide coating on nickel substrate by metal organic chemical vapor deposition. *Surface & Coatings Technology*, 173, pp. 74-80.
- Peng, X. (2009). Nanoscale assembly of high temperature oxidation resistant nanocomposites. *Nanoscale*, 2, pp. 262-268.
- Providing Challenging Ultrasonic Solutions. (2002). *Basic Elements of MMM Systems & How MMM Systems Operate*. MPInterconsulting.
- Putrasari, Y. (2011). *Preparation of NiO Catalyst on FeCrAl Substrate Using Various Techniques at Higher Oxidation Process*. Universiti Tun Hussein Onn Malaysia: Master's Thesis.
- Reszka, K., Morgiel, J. & Reszka, J. (2006). Structure and properties of an alumina/amorphous-alumina/platinum catalytic system deposited on FeCrAl steel. *Journal of Microscopy*, 224, pp. 46-48.
- Rose, I. & Whittington, C. (2002). *Nickel Plating Handbook*. Finland: OM Group.
- Santos, H. & Costa, M. (2008). Evaluation of the conversion efficiency of ceramic and metallic three way catalytic converters. *Energy Conversion & Management*, 49, pp. 291-300.
- Sebayang, D., Putrasari, Y., Hasan, S. & Untoro, P. (2010). NiO development on FeCrAl substrate for catalytic converter using ultrasonic and nickel electroplating methods. *Advanced Material Research Journal*, 129-131, pp. 1262-1266.

- Stefanescu, A., Veen, A. C. V., Brunel, E. D. & Mirodatos, C. (2007). Investigation of Ni-based steam reforming catalyst developed for the coating of microstructures. *Chemical Engineering Science*, 62, pp. 5092-5096.
- Sun, H., Quan, X., Chen, S., Zhao, H. & Zhao, Y. (2007). Preparation of well-adhered  $\gamma$ -Al<sub>2</sub>O<sub>3</sub> washcoat on metallic wire mesh monoliths by electrophoretic deposition. *Applied Surface Science*, 253, pp. 3303-3310.
- Suslick, K. S. (2000). *The Chemistry of Ultrasound*. Chicago: Suslick Research Group Chemistry University of Illinois.
- Valentini, A., Carreno, N. L. V., Leite, E. R., Goncalves, R. F., Soledade, L. E. B., Maniette, Y., Lengo, E. & Probst, L. F. D. (2004). Improved activity and stability of Ce-promoted Ni/ $\gamma$ -Al<sub>2</sub>O<sub>3</sub> catalysts for carbon dioxide reforming of methane. *Latin American Applied Research*, 34, pp. 165-172.
- Valentini, A., Carreno, N. L. V., Probst, L. F. D., Lisboa Filho, P. N., Schreiner, W. H., Leite, E. R., & Longo, E. (2003). Role of vanadium in Ni:Al<sub>2</sub>O<sub>3</sub> catalysts for carbon dioxide reforming of methane. *Appl. Catalysis A: General*, 255, pp. 211-220.
- Valentini, M., Groppi, G. & Cristiani, C. (2001). The deposition of  $\gamma$ -Al<sub>2</sub>O<sub>3</sub> layers on ceramic and metallic supports for the preparation of structured catalysts. *Catalysis Today*, 69, pp. 307-314.
- VBulletin Solutions Inc. (2011). *Metal Substrate*. Retrieved Nov 7, 2010.
- Wei, Q., Chen, Z. X., Nie, Z. R. & Hao, Y. L. (2005). Mesoporous activated alumina layers deposited on FeCrAl metallic substrates by an in situ hydrothermal method. *Alloys and Compounds*, 396, pp. 283-287.
- Wu, X., Weng, D., Xu, L. & Li, H. (2001). Structure and performance of  $\gamma$ -alumina washcoat deposited by plasma spraying. *Surface & Coatings Technology*, 145, pp. 226-232.

- Wu, X., Weng, D., Zhao, S. & Chen, W. (2005). Influence of an aluminized intermediate layer on the adhesion of a  $\gamma$ -Al<sub>2</sub>O<sub>3</sub> washcoat on FeCrAl. *Surface & Coatings Technology*, 190, pp. 434-439.
- Yang, K. S., Jiang, Z. & Chung, J. S. (2003). Electrophoretically Al-coated wire mesh and its application for catalytic oxidation of 1,2-dichlorobenzene. *Surface & Coatings Technology*, 168, pp. 103-110.
- Young, D. J. (2008). *High Temperature Oxidation and Corrosion of Metals*. 1<sup>st</sup> ed. Amsterdam: Elsevier.
- Zeng, S. H., Liu, Y. & Wang, Y. Q. (2007). CuO-CeO<sub>2</sub>/Al<sub>2</sub>O<sub>3</sub>/FeCrAl monolithic catalysts prepared by sol-pyrolysis method for preferential oxidation of carbon monoxide. *Catalysis Letters*, 117, pp. 119-126.
- Zhao, S., Zhang, J., Weng, D. & Wu, X. (2003). A method to form well adhered  $\gamma$ -Al<sub>2</sub>O<sub>3</sub> layers on FeCrAl metallic supports. *Surface & Coatings Technology*, 167, pp. 97-105.